Papers of Ship Research Institute Vol.31 No.1 Technical Report

Nonlinear Response of Moored Floating Structures in Random Waves and its Stochastic Analysis

Part 2 Comparison among Simulations, Statistical Predictions and a Full Scale Measured Data

By

Shunji KATO*, Masakatsu SAITO* and Satoru TAKASE**

Abstract

This paper deals with a simulation and statistical prediction of total second order responses, including slow drift motions caused by waves and wind, of a full scale floating offshore structure "POSEIDON". The at-sea experiment was carried out from June, 1986 to July, 1990 at the Japan Sea. Firstly, we develop a new analysis method based on time series fitting using a nonlinear optimization technique in order to study the hydrodynamic and restoring force characteristics from full scale free decaying test data. Secondly, in order to investigate the second order force characteristics and the contribution of wind fluctuations to slow drift motions, we carry out not only the cross bi-spectral analysis of motion and waves but also the multi-input analysis of motion, waves, instantaneous wave power and wind fluctuations. Furthermore, with respect to the second order forces, a comparison between analyzed results and numerical ones calculated by the potential theory is made.

On a basis of these investigations, a comparison between a measured time history of slow drift motion and simulations is carried out.

Relating to statistical estimates of the PDF(Probability Density Function) and the extreme response, a new prediction method is developed to take account of both second order wave forces and varying wind loads.

At-sea measured sample data, the statistical prediction based on the Rayleigh distribution, i.e. the so-called *Cartwright-Longuet-Higgins'* estimates and the results obtained from the present method are compared. Main results are as follows:

1) The present method analyzing free decaying data is effective to get the drag coefficient depending on the K-C number (*Keulegan-Carpenter* number). In this case, the drag coefficient of surge and sway motions can be described as sum of a constant term and a K-C dependent term, which is inversely proportional to the K-C number. And the constant term of the full-scale structure is as same as that of model while the K-C dependent term of the full-scale structure is larger than that of model.

2) In order to simulate slow drift motions, not only in-line wind fluctuations but also transverse ones should be taken into account even though the mean wind direction is head. As a wind spectrum representing wind fluctuations, a spectrum

*Ocean Engineering Division
**Hiroshima University
Received on May 6, 1993

form with significant power in low frequency compared with the well-known Davenport and Hino spectra (suggested by *Ochi-Shin* and *Kato*) should be used.

3) As for estimation of the second order slow drift force, not only the potential drift force but also viscous drift force should be taken into account.
And the comparison between the time domain simulation and the measured result supports the usefulness of the present model consisting of the two term Volterra series model to wave process plus the linear response model to wind fluctuation process. However, the problems of the phase of QTF of second order force and the wave drift damping remain unsolved.

4) The probability distribution estimated from the present method agrees very well with the measured one. And as for the estimation of extreme response, it is confirmed that the *Cartwright-Longuet-Higgins'* estimate affords the significant underestimation of the measured results while the present method slightly overestimates them.

1. Introduction

One of the major considerations in the design of an offshore mooring system is the large amplitude slow drift motions which may be exhibited by the moored structure. It is said that these motions are a resonant response to nonlinear low frequency second order wave force and low frequency wind force. Although the response of the structure may be considered to be second order dominated, the contribution of the wind and first order wave forces can significantly effect on the response of the structure and should therefore be included within the analysis.

For the case of a linear mooring system a technique originally proposed by *Kac* and *Siegert* [1] provides a suitable procedure for determining an analytical expression for the characteristic function of the combined response. The probability density function of the response is then given by the Fourier transform of the characteristic function.

Naess [2, 3] has shown that it is possible to derive an analytical expression for the probability density function (PDF) of the pure second order component of the response. However, a closed form expression for the PDF of the combined first and second order response does not appear to be available.

Alternatively, *Kato* and *Kinoshita* [4] have developed an approximate method. This method is based on generalised Laguerre polynomials and has been used to calculate the combined distribution, where technique leads to an expression for the PDF in the form of a convolution integral.

Furthermore they have shown from the comparison between the model test and the estimation results that the approximate method is useful to get the response statistics of slow drift motions of moored offshore structures.

Up to now, a number of papers have been presented relating to the response statistics of the slow drift motion of offshore structures. However, these papers have been limitted to theoretical and model experimental researches. There is few papers dealing with

the correlation among the full scale measurements, numerical predictions and model test results.

In this paper, we deal with a simulation and statistical prediction of total second order responses, including slow drift motions caused by waves and wind, of a prototype floating offshore structure. We show the correlation among the full-scale measurements, the model test results and the estimation ones.

We carried out the at-sea experiment using a prototype floating platform "POSEIDIN" from September, 1986 to July, 1990. One of the most important research themes in this project was a study of predicting maximum excursions of slow drift motions and mooring forces.

In chapter 2, we show the outline of such project and the data acquisition system of motions and environmental conditions.

In chapter 3, fundamental characteristics of hydrodynamic and static restoring forces of the "POSEIDON" are presented.

In order to investigate them, full scale free decaying tests were carried out during the at-sea experiment. For analyzing this data, a new method, which is based on time series fitting using a nonlinear optimization technique, is developed. By using this method, the hydrodynamic coefficients, especially the drag coefficient and the stiffness coefficients of full-scale structure are found out. Furthermore the scale effect of drag coefficient is studied through a comparison between model test results and the analysis ones of at-sea data.

In chapter 4, the second order force characteristics and the contribution of wind fluctuations to slow drift motions are investigated and the comparison between numerical simulations and measurements is carried out.

Not only the cross bi-spectral analysis of motion and waves but also the multi-input analysis of motion, waves, instantaneous wave power and wind fluctuations is carried out. With respect to the second order forces, a comparison between analyzed results and numerical ones calculated from the potential theory is also done.

On the basis of these investigations, we compare a measured time history of slow drift motion with simulations.

In chapter 5, relating to statistical estimates of the PDF (Probability density function) and the extreme response, a new prediction method is developed to take account of both second order wave forces and varying wind loads.

At-sea measured sample data, the statistical prediction based on the Rayleigh distribution, i.e. the so-called *Cartwright-Longuet-Higgins'* estimates and the results obtained from the present method are compared.

In chapter 6, the conclusions are summarized as follows.

- The present method to analyze free decaying data is effective to get the drag coefficient depending on the K-C number (*Keulegan-Carpenter* number) . In this case, the drag coefficient of surge and sway motions can be described as sum of a constant

term and a K-C dependent term, which is inversely proportional to the K-C number. And the constant term of the full-scale structure is as same as that of model while the K-C dependent term of the full-scale structure is larger than that of model.

- In order to simulate slow drift motions, not only in-line wind fluctuations but also transverse ones should be taken into account even though the mean wind direction is head. As a wind spectrum representing wind fluctuations, a spectrum form with significant power in low frequency compared with the well-known Davenport and Hino spectra (suggested by *Ochi-Shin* and *Kato*) should be used.

- The probability distribution estimated from the present method agree very well with the measured one. And as for the estimation of extreme response, it is found that the Cartwright-Longuet-Higgins' estimate affords the significant underestimation of the measured results while the present method slightly overestimates them.

2. Outline of at-sea experiment

Concerning the outline of this experiment, we have reported a number of papers. The details are referred to other papers, e.g. *Ohmatsu et al* [5]. In this paper, we describe it briefly.

2.1 Floating test structure "POSEIDON"

The test structure used is named "POSEIDON", which means Platform for Ocean Space Exploitation. The structure is shown in Fig.2.2. It consists of twelve legs with footings which support the upper structure, which is mainly composed of the box type girders around four sides. The instrumentation house is arranged on the upper deck for power supply and data acquisition.

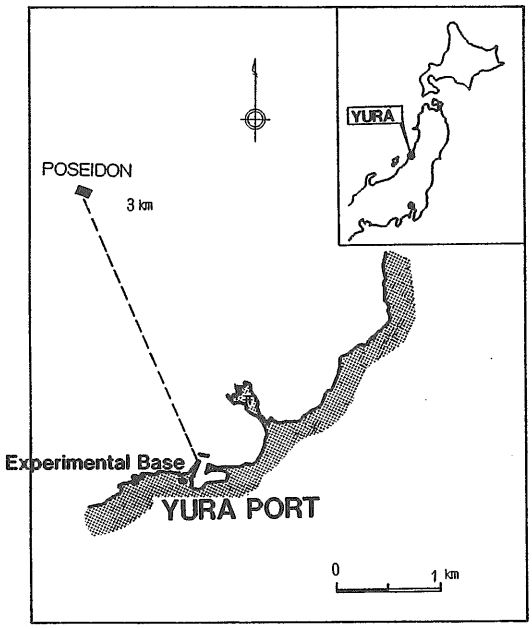

Fig. 2.1 Test field of At-sea experiment

2.2 Location of test area

The location of test area is about 3 km offshore Yura port, Tsuruoka-city, Yamagata Prefecture, southwestern part of the Japan Sea as shown in Fig.2.1. The water depth is about 41 m. In winter we have seasonally severe sea conditions caused by the strong wind. The POSEIDON was constructed at Naruto, Tokushima Prefecture. After an inclining and free decaying test, it was towed by a tag boat from Naruto port to Yura port, about 800 miles over 9 days, and installed in the test area of Yura port in July, 1986.

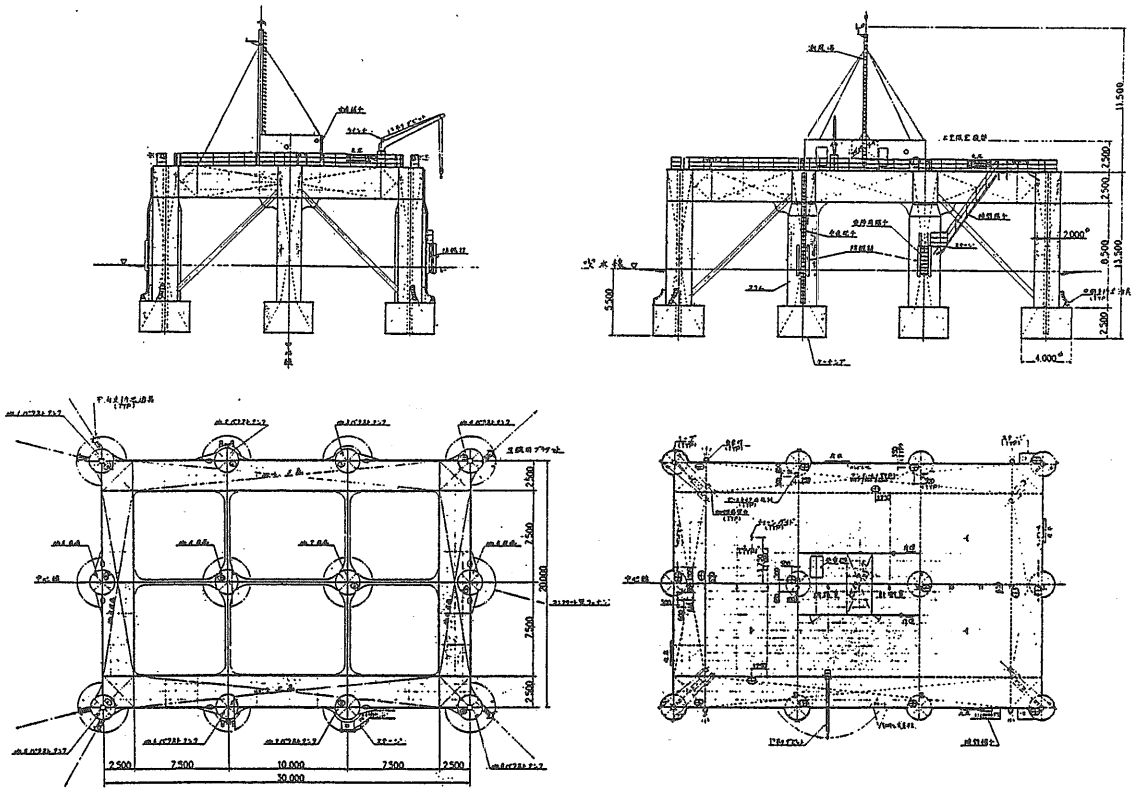

Fig. 2.2 Structural configuration of the prototype structure "POSEIDON"

The POSEIDON was slackly moored by six chain lines as shown in Fig.2.3. The forward direction was WNW, which corresponds to the dominant direction of seasonal wind and waves in winter.

2.3 Measurements

The POSEIDON has many measuring items. They are shown in Table 2.1. Now, we shall explain briefly the main items, i.e. wave, wind, wind pressure, slow drift motion measurements.

2.3.1 Wave measurement

Three ultrasonic wave probes were installed as a line array on the bottom of 180 m offshore of the POSEIDON (see Fig.2.3). They were used to estimate directional wave spectra. And measured data were used for the linear magnitude of unidirectional incident waves required in the following simulation. At the same time, we also measured a relative water level and vertical acceleration at the centre column of offshore side. Those data were used as a phase information for simulating unidirectional incident waves.

Table 2.1 Measuring items and devices

ITEMS	No.	Devices and Remarks
Wind	2	Ultrasonic, 3 axes, 19. 5m above W. L. Ultrasonic, 1 axes, 10. 0m above W. L.
Waves	3	Ultrasonic, sea floor of 180 m offshore of POSEIDON line array
Current	1	Impeller type, under 10 m below W. L.
Temparature air	1	Resistance temparature type, on the top of hous
Temparature water surface	1	Semiconductor type, at the footing
Temparature bottom	1	Semiconductor type, on the sea floor
Humidity	1	Thin film capacitive type, on the top of house
Solar radiation	1	Thermopile type, on the top of the house
Temparature deck plate	1	Resistance temparature device
Temparature house wall	1	Resistance temparature device
Relative water level	1	Ultrasonic, at the centre column of offshore side
Impact pressure	3	Strain type, 1m, 3m and 6m above W. L. on the center column of offshore side
Wind pressure	2	Semiconductor sensor, difference of wind pressures on fore & aft side of upperstructure and starboad & port side of upperstructure
Acceleration	5	servo type, surge, sway and heave (center, fore and aft)
Roll	1	Vertical gyroscope
Pitch	1	Vertical gyroscope
Yaw	1	Directional gyroscope
Slow drift motion	6	Ultrasonic, 2 transmitters on the footings and 3 receivers on the sea floor
Mooring line tension	8	Load cell type, strain gauge type
Strain	12	Strain gauge installed indirectly

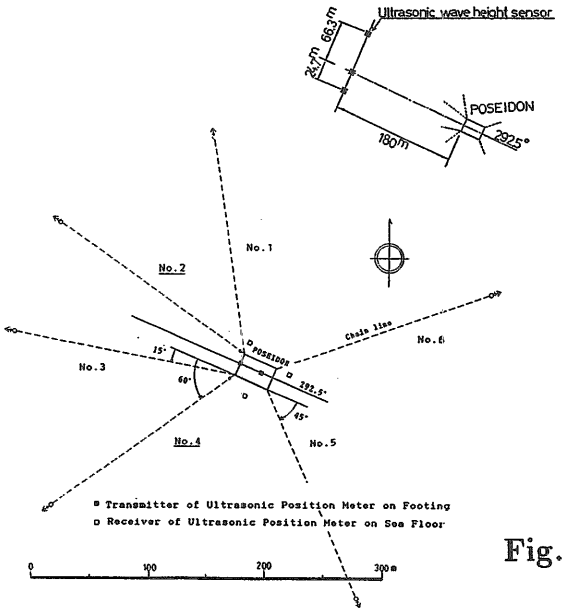

Fig. 2.3 Set-up of mooring system and wave measurement system

2.3.2 Wind and wind pressure measurements

An ultrasonic type three axes anemometer was installed at the top mast, which is 19.5m height above sea surface. It was used to measure mean and fluctuating wind velocities in three directions (directions of surge, sway and heave motion). The response time of this anemometer is 0.5 Hz.

Wind pressures were measured by using difference pressure sensors installed on fore & aft side and starboard & port side of upper structure (see Fig.2.4). Each pressure holes are led to two semiconductor type difference pressure sensors through tubes.

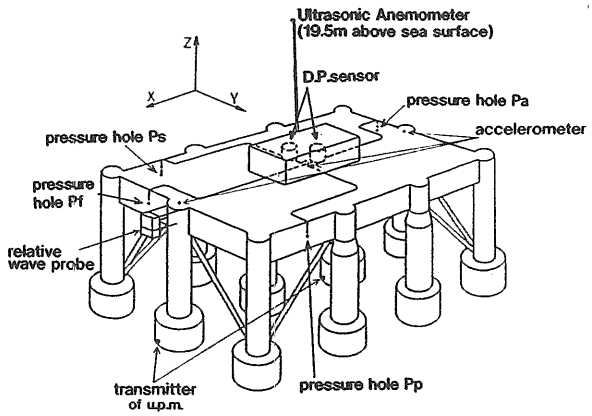

Fig. 2.4 Wind pressure measurement system

Concerning mean wind pressures, Fig. 2.5 compares the measured result with the model test result. Both results are in good agreement. It is found from this figure that the pressure coefficient C_p is about 1.3. Figure 2.6 shows a comparison between an example of the measured time history of wind pressure time history in surge direction and that estimated from wind fluctuation in the same direction by the following relation

$$\bar{p} + p = \frac{1}{2}\rho_a C_p (\bar{U} + u)^2$$
$$\bar{p} = \frac{1}{2}\rho_a C_p \bar{U}^2$$
$$p \sim \rho_a C_p \bar{U} u$$

where ρ_a is the air density, $\bar{U}$ is the measured mean wind velocity in surge direction.

From this figure it is found that fluctuating wind pressure and wind velocity have one-to-one correspondence.

2.3.3 Measurement of slow drift motion

A new in-situ measurement system of a slow drift motion was developed in the preliminary investigations. It consists of two ultrasonic type transmitters and three receivers. The transmitters were installed on the footings of POSEIDON and receivers were located on the sea floor of 41 m water depth as shown in Fig.2.7. Since distances between transmitters and receivers are measured successively by using the triangle quadrature method, we could obtain time series of six mode motions. At the same time, first order motions were measured by three axes servo-type accelerometers and vertical and directional gyroscopes settled on the centre of POSEIDON.

Figure 2.8 shows an example of measured time history of surge motion and a comparison between its filtered one, raw data of which were measured by this new measuring system,

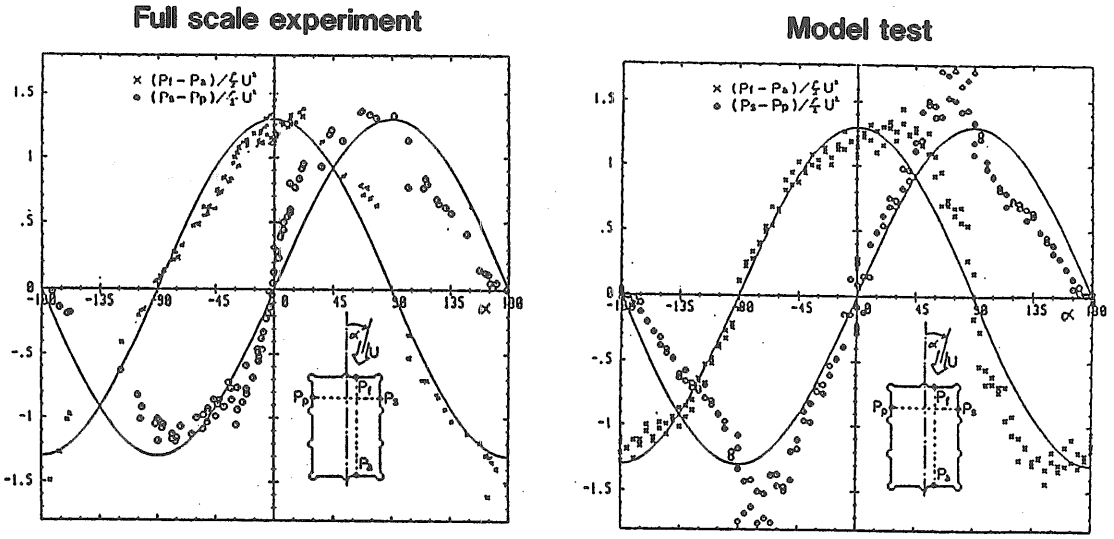

Fig. 2.5 Comparison between model test result and full-scale measuremt with respect to mean wind pressure distribution

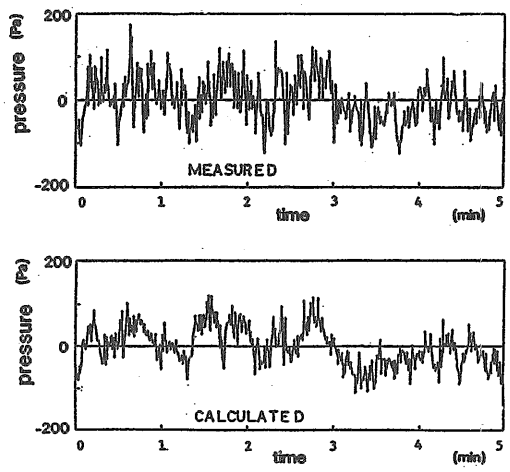

Fig. 2.6 Comaprison between measured and simulated results with respect to wind pressure fluctuation

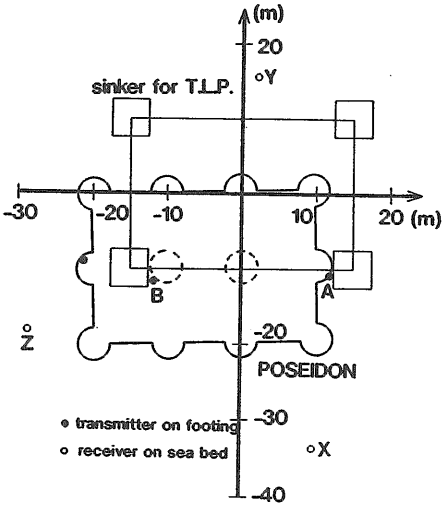

Fig. 2.7 Position measuring system by use of ultrasonic wave

and that measured by the servo type horizontal accelerometer. The measuring device has a function removing the angular motion effects. A mimimum frequency was 1/25 Hz. It is found that the accuracy of this system is excellent.

2.4 Data acquisition system

Forty eight items are automatically recorded by a personal computer every six hours. One record time was 34 minutes and 8 seconds. The sampling interval was 0.5 sec. thus 4096 data are recorded for each item.

In order to record a long duration data, another recording system is also used. The system is that the long duration measurement can be started by a command of telemeter system. In this case, the sampling interval was 1.0 sec. The records were stored into the on board hard disc of 40 MB.

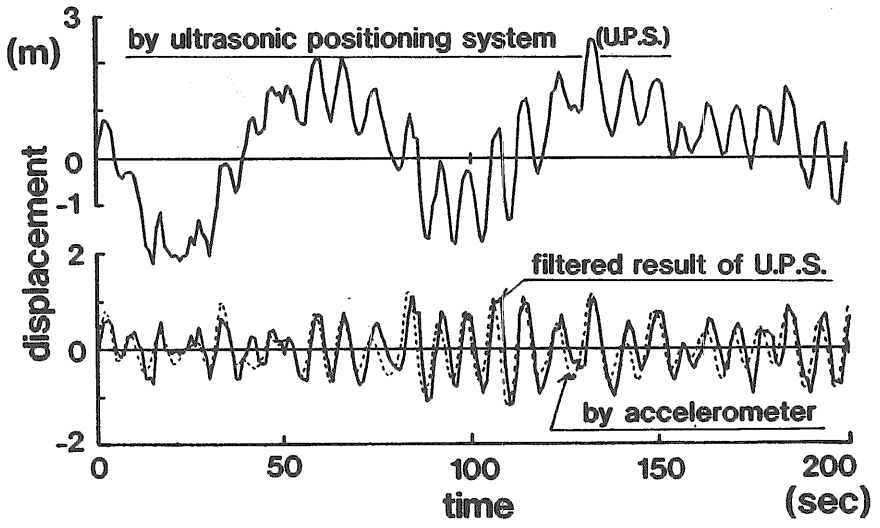

Fig. 2.8 Comparison of measured surge time histories between by accelerometer and by ultrasonic type position measurering system

3. Measured results

3.1 Slow drift motion due to wind

Figure 3.1 shows time histories of wind velocity, wind pressure difference and sway motion. Environmental conditions at that time were as follows; the mean wind velocity was 13.8 m/sec, the mean wind direction was 104° from Fore to Port, significant wave height was 0.3 m, and current speed was less than 0.5 m/sec.

This situation is a typical case that wind is dominant.

From this figure it is found that there exists a very long fluctuation component in sway motion time history. And it seems that the time history of such fluctuation corresponds to one of wind velocity fluctuation. To confirm this fact, a simple coherency analysis was carried out. Figure 3.2 indicates an example of a result of coherency analysis. As for frequency components lower than 0.01 Hz, wind pressure fluctuation and slow drift motion of sway lie in a linear correlation and the phase of frequency transfer function between them is about 0 degree., i.e. the wind pressure and slow drift motion of sway exactly correspond.

3.2 Slow drift motion due to wind and waves

Since a datum assumed stationary in statistical sense, the data (9 hours duration) shown in Fig.3.3 were adopted and analyzed to study how much wind and waves contribute to the slow drift motion. Mean wind and mean wave directions were about head as found in Fig.3.3. Mean values of significant wave height and significant mean period are 3.0 m and

7.0 sec. respectively. Figure 3.4 shows spectra of waves, surge and sway motions. As a spectral analysis, the AR(Auto Regression) model method was used and the order of AR model was determined on the basis of least Akaike Information Criteria principle.

There exist three peaks in the surge spectrum in Fig.3.4. The first lies in the vicinity of wave frequency 0.12 Hz, the second is in 0.07 Hz and the last is in 0.0156 Hz (64 seconds in period). It seems that the last one is not recognized in the sway spectrum. The first peak in the surge and sway spectra is due to waves and the second one is due to coupling motions since they agree with the natural frequencies of roll and pitch motions.

Figure 3.5 shows time histories of surge, sway and wind pressure differences. The time history of sway motion and the one of wind pressure difference in sway direction are in good agreement but the surge motion is not in accordance with the wind pressure difference in surge direction. Figure 3.6 shows a simple coherency between sway motion and wind pressure difference in sway direction. It is found that the slow drift motion of sway occurs even if the mean wind velocity direction lies in the surge direction and it is caused by the wind pressure difference in sway direction, i.e. transverse wind fluctuation. Figure 3.7 shows the wind spectra in surge direction (the direction of mean wind velocity) and sway direction (transverse direction). From this figure, wind spectral intensity in sway direction has the same order as one of surge direction. Spectral peak frequencies of non-dimensional wind spectra in both directions

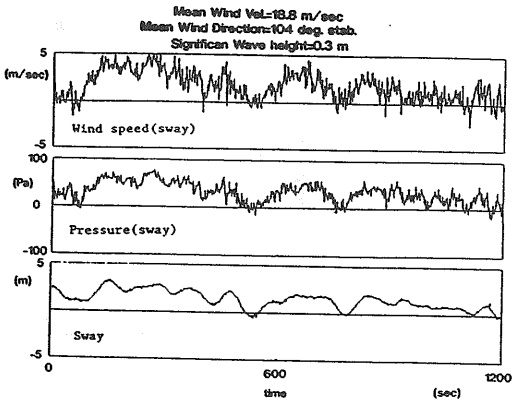

Fig. 3.1 An example of wind velocity, wind pressure fluctuation and time histories of sway under a wind dominant condition

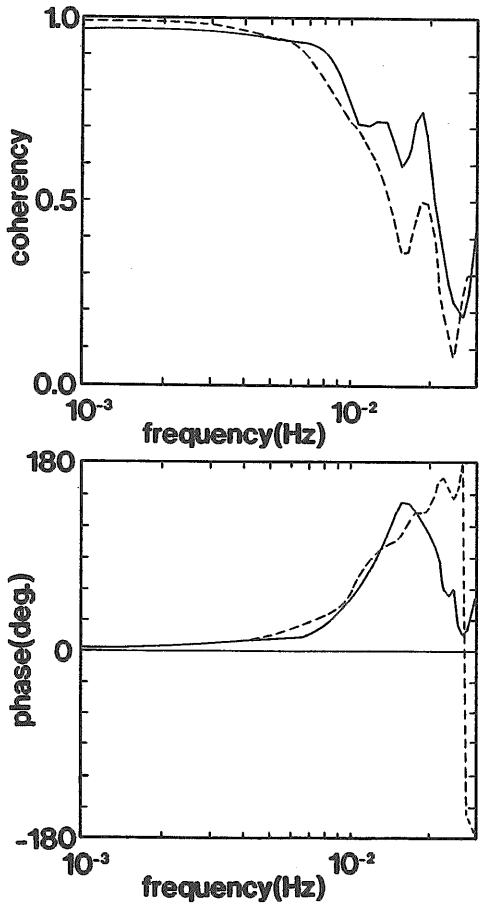

Fig. 3.2 Coherency and phase between transverse wind pressure fluctuation and sway motion

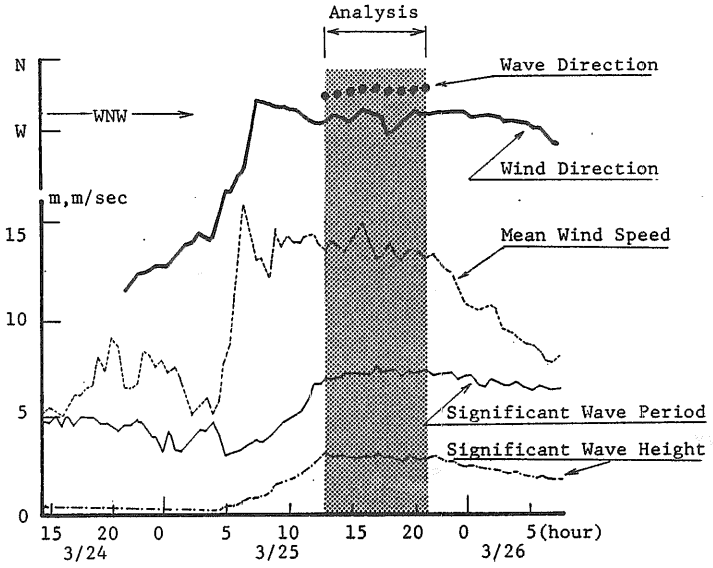

Fig. 3.3 A time history of statistical values of waves and wind (The shaded portion is intended for investigation)

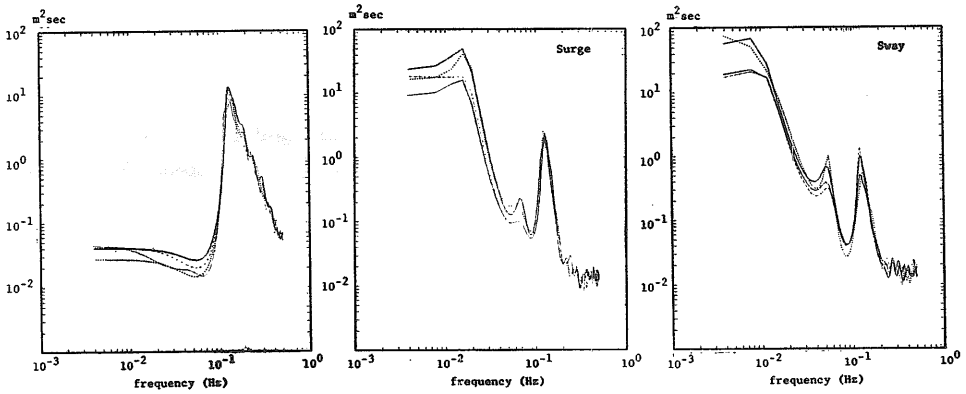

Fig. 3.4 Examples of wave, surge and sway spectra

downshift compared with ones of representative spectra, e.g. Davenport and Hino spectra, representing wind spectra over land. And measured spectra are close to a spectrum form suggested by *Kato* [7]. Moreover, the fact that wind spectrum over sea has more significant power in low frequency than that over land has recently been measured in the world. *Ochi and Shin* [6] have suggested a new spectrum on the basis of mean value of main wind spectra measured over sea surface. And *Kato et al.* [7] have also suggested a new wind spectrum form based on both physical investigations and the measurement at the Japan Sea. Figure 3.8 shows a comparison of wind spectra among Ochi and Shin's formula, the author's one and the other spectrum forms under a typical strong wind condition. Our

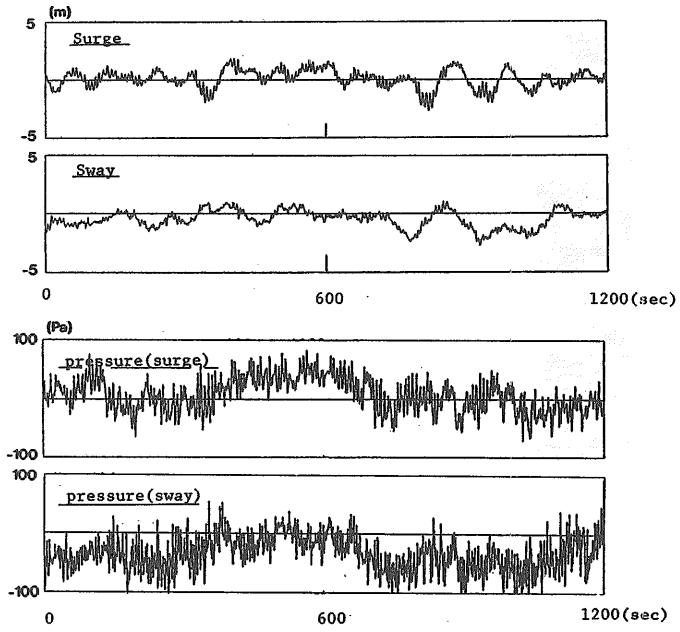

Fig. 3.5 Time histories of surge, sway and wind pressure fluctuations in surge and sway directions

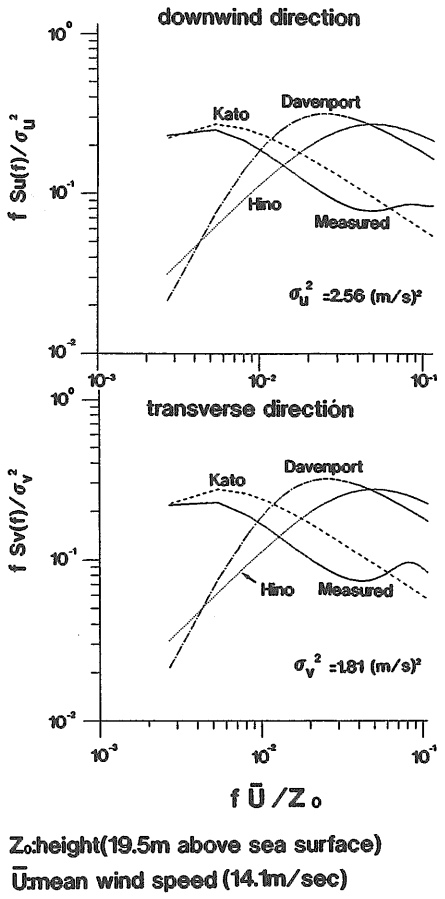

Zo:height(19.5m above sea surface)
Ū:mean wind speed (14.1m/sec)

Fig. 3.7 An example of wind velocity spectra in sway and surge directions (σ_u^2 and σ_v^2 are the wind velocity powers in downwind and transverse directions respectively. The horizontal axis means wind frequency and the vertical axis represents the nondimensional wind velocity spectrum)

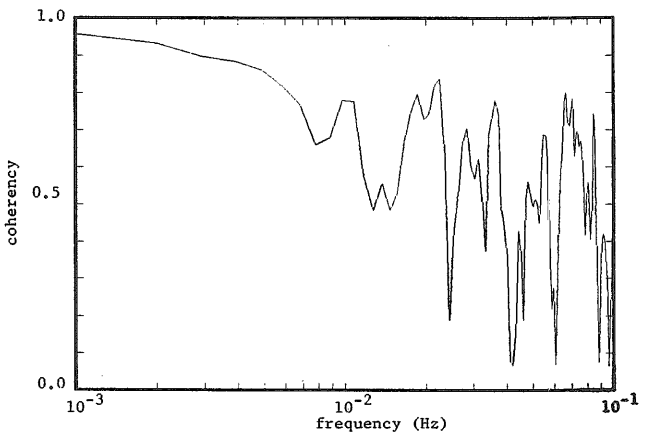

Fig. 3.6 Coherency between sway motion and wind pressure fluctuation in sway direction

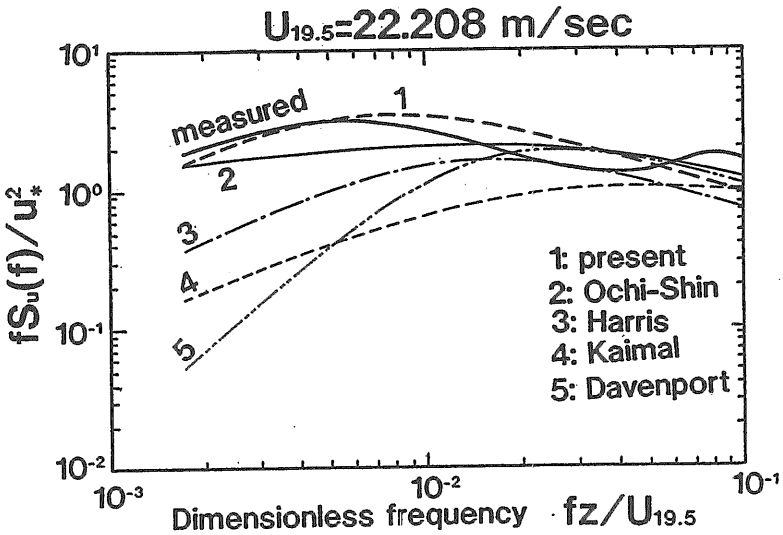

Fig. 3.8 Comparison between measured wind spectrum and other proposed spectrum forms
(u_* means the friction velocity over sea and it is in proportion to the standard deviation of wind velocity fluctuation)

data subject to this comparison is one hour data where the mean wind velocity was 22.208 m/sec. In this figure, heavy solid line indicates the measured spectrum, heavy broken line is the estimated one by the author and thin lines are the typical spectrum forms, cited by *Ochi et al.* This figure shows that the measured spectrum agrees very well with the author's one and it is close to the Ochi-Shin's spectrum.

In this way, we found that wind spectrum over sea is different from one over land and the former has a significant low frequency power compared with the latter. And even if the mean wind velocity direction and the direction of surge are same, wind spectrum in sway direction is significant and it has the same power as one in surge direction.

Furthermore, we should note that the transverse wind fluctuation, i.e. varying wind velocity in sway direction, possibly causes a slow drift motion in the sway direction.

While from Fig.3.5 it seems that the slow drift motion in the surge direction is caused by both waves and wind fluctuation.

Hence, in order to investigate how much each environmental excitations contribute to the surge slow drift motion, we carried out a multiple input analysis.

The concept and analysis procedure of multiple input have been shown by *Tick* [8] and others. *Yamanouchi* [9] applied it to the transverse stress of ship in random waves.

The concept of multi-input analysis is as follows:

If we assume that the surge motion process can be expressed as a linear output process $y(t)$ of many environmental excitation processes $x_i(t)$, *e.g.* x_1 is the surface elevation, x_2 is the instantaneous wave power and x_3 is the wind velocity fluctuation, in the following

equation:

$$y(t) = \sum_i \int h_i(\tau) x_i(t-\tau) d\tau \tag{3.1}$$

then the auto correlation and spectrum of the output process are given by:

$$R_{yy}(\tau) = \sum_{i=1}^{n} \sum_{j=1}^{n} \int h_i(\alpha) h_j^*(\beta) R_{ij}(\alpha - \beta + \tau) d\alpha d\beta \tag{3.2}$$

$$S_{yy}(f) = \sum_{i=1}^{n} \sum_{j=1}^{n} H_i(f) H_j^*(f) S_{ij}(f) \tag{3.3}$$

where $H_i^*(f)$ is the complex conjugate function of the response function$H_i(f)$ and $H_i(f)$ is the Fourier transform of h_i. And the cross spectrum to the input x_j is

$$S_{yj}(f) = \sum_{i=1}^{3} H_i(f) S_{ij}(f) \tag{3.4}$$

where $R_{ij}(\tau)$ and $S_{ij}(f)$ are the cross correlation function and cross spectrum between inputs respectively.

Here the second order forcing process $f_d(t)$ can exactly be expressed as

$$f_d = \int \int g_2^f(\tau_1, \tau_2) x_1(t-\tau_1) x_1(t-\tau_2) d\tau_1 d\tau_2$$

However, it is equivalent to the following equation in sense of stochastic process (see *Kato et al.* [19]):

$$f_d = \int h_2(\tau) x_1^2(t-\tau) d\tau$$

This implies that the second order forcing process f_d can be represented by a linear response to instantaneous wave power, i.e. $x_2 = x_1^2$, where all input processes x_i are stationary and their mean values are eliminated in advance.

Now, by putting $\mathbf{x}(t) = [x_1(t), x_2(t), x_3(t)]$ and

$$\mathbf{H}(f) = [H_1(f), H_2(f), H_3(f)], \tag{3.5}$$

$$\mathbf{S}_{xx}(f) = \begin{bmatrix} S_{11}(f) & S_{12}(f) & S_{13}(f) \\ S_{21}(f) & S_{22}(f) & S_{23}(f) \\ S_{31}(f) & S_{32}(f) & S_{33}(f) \end{bmatrix} \tag{3.6}$$

Eq.(3.3) is represented as follows:

$$S_{yy}(f) = \mathbf{H}(f) \mathbf{S}_{xx}(f) \mathbf{H}^{*\prime}(f) \tag{3.7}$$

where $\mathbf{H}^{*\prime}(f)$ means a complex conjugate function of $\mathbf{H}(f)$ and "$\prime$" denotes the transpose matrix.

While since

$$\mathbf{S}'_{yx}(f) = \mathbf{S}_{xx}(f) \cdot \mathbf{H}'(f)$$

from Eq. (3.4), a three dimensional frequency response function is given as:

$$\mathbf{H}'(f) = \mathbf{S}_{xx}^{-1}(f) \cdot \mathbf{S}'_{yx}(f) \qquad (3.8)$$

In the case of single-input/single output system, a simple coherency function representing the degree of linearity between input and output can be defined as usual. In the same way, a coherency function can also be defined in the case of multi-input/single-output system. It is called the multiple coherency, which is represented in the following form:

$$\begin{aligned} \hat{\gamma}^2_{yx}(f) &\equiv \hat{\gamma}^2_{y,123}(f) \\ &= \frac{1}{S_{yy}(f)} \mathbf{H}(f) \mathbf{S}^{*\prime}_{yx}(f) \end{aligned} \qquad (3.9)$$

And by using the concept of conditional spectrum proposed by *Tick* [8], the partial coherency is given by:

$$\hat{\gamma}^2_{yi,j}(f) = \frac{|S_{yi,j}(f)|^2}{S_{ii,j}(f) S_{yy,j}(f)} \quad (i,j = 1,2,3) \qquad (3.10)$$

where the partial coherency function $\hat{\gamma}^2_{yi,j}$ means the coherency between the output $y(t)$ and an input $x_j(t)$ after all of the linear correlation part between $y(t)$ and the inputs $x_i(t)(i \neq j)$ were removed. And $S_{ii,j}(f), S_{yy,j}(f)$ and $S_{yi,j}$ are the conditional auto spectra and the conditional cross spectrum respectively.

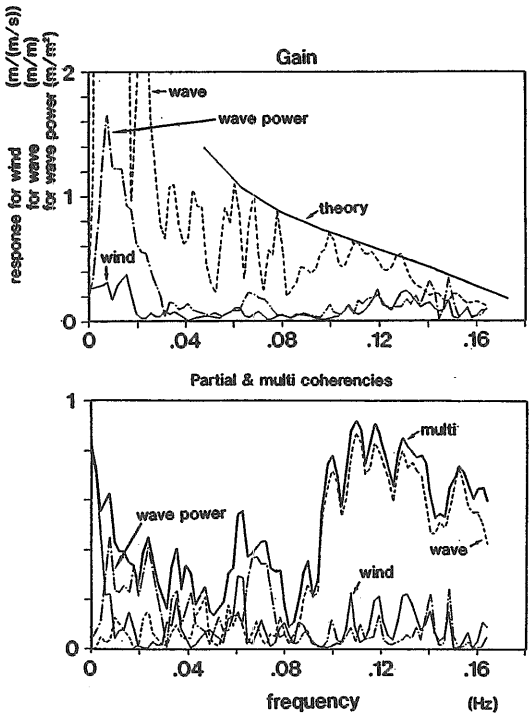

Fig. 3.9 Gains of frequency response function, partial and multiple coherencies among surge motion and wave, instantaneous wave power and wind pressure fluctuation in head sea and wind
(The "theory" in the upper figure means the the calculated line based on the first order potential theory and the "multi" in lower figure represents the multi coherency)

Using such a definition of conditional spectra, the frequency response function of the output $y(t)$ to an input $x_i(t)$ can be represented in the following form [8]:

$$H_i(f) = \frac{S_{yi,j}(f)}{S_{ii,j}(f)} \qquad (i,j = 1,2,3) \qquad (3.11)$$

The upper graph of Fig.3.9 shows the gain of H_i. This represents the frequency response functions for each external excitations. The thin broken, dash-dotted and solid lines indicate the responses for waves, instantaneous wave power and wind velocity respectively.

The bold solid line represents the numerical calculation obtained by the linear motion theory. The lower graph of Fig.3.9 shows the partial coherencies and the multiple coherency among surge motion process and external excitations. In this figure there exist two frequency regions indicating high values of the multiple coherency. The one region is higher than 0.1 Hz and another is lower than 0.01 Hz. Since the partial coherency between surface elevation and surge motion shows a high value in the former region, the surge response higher than 0.1 Hz is caused by wave surface elevation. While, it is considered that two excitations contribute to the surge response in low frequencies lower than 0.01 Hz. Wind excitation contributes to the surge response in very low frequencies lower than 0.005 Hz and instantaneous wave power, which corresponds to wave drift excitation because square of wave height is in proportion to wave drift force, does to the surge motion in frequency range from 0.005 Hz to 0.01 Hz

Next, we shall verify this result due to time domain simulations.

4. A comparison between a time domain simulation and a measured time history

4.1 Determination of hydrodynamic force and stiffness coefficients

4.1.1 Determination by numerical calculation

The added mass and wave radiation damping coefficients were calculated using the three dimensional source distribution method. In the computation the mean wetted surface of the body was approximated by 640 facets. In order to get the so-called memory effect function which is needed to solve the equation of motion in time domain, we used the approximate calculation method. Namely, we extrapolated the wave radiation damping, which was obtained in advance in some frequency range, by using the spline function, then found a frequency ω_0 which the extrapolated value becomes zero, and calculated the finite integral over $\omega_0 \geq \omega \geq 0$ instead of infinite integral.

In order to check the accuracy of its approximate calculation, we compared the results with theoretical asymptotic ones.

Takagi and Saito [10] showed theoretically an asymptotic behavior of the memory effect functions for a half submerged sphere. Comparisons between their results and the present calculations were carried out (see the reference [4]) and then it was found that both results were in good agreement except for a slight discrepancy to the calculated memory effect function. However, it may be considered that the present approximation is accurate enough from practical point of view to get memory effect functions since in general radiation damping forces exponentially decrease with increasing oscillation frequency; *e.g. Kato et al.* [4]. We should note that the added mass is slightly modified by the truncation effect. In this case, calculations were carried out up to the frequency range such that a stable added mass can be obtained in the time domain motion equation.

4.1.2 Determination by experiments

At-sea experiment

In order to find out the hydrodynamic force coefficients of a full-scale offshore structure, free decaying tests using the POSEIDON were carried out in July, 1990. Table 4.1 shows the content of the experiment.

Model tests

Two kinds of model experiment were also carried out. The one is a forced oscillation test, and another is a free decaying test. The model size is 1/25 of the full scale structure. Six mooring chain lines were set under the same condition as the at-sea experiment shown in Fig.2.3. The chain weight per unit length in water was 75 gf/m and the water depth was 1.664m. The mass of the structure excluding mooring chain masses was 31.3 kg and values of the radius of gyration in pitch and roll motions were 400 mm and 530mm respectively.

Initial displacements of free decaying tests were 20 cm for surge and 12 cm for sway. Table 4.2 indicates β values, i.e. the ratio between *Reynolds* number (*Re* number) and *Keulegan-Carpenter* number (K_c number), at the at-sea and model decaying tests. As a representative length for a definition of Reynolds and K_c numbers, we used the diameter of one column, i.e. 0.12 m.

Table 4.1 Experimental conditions of full-scale free decaying test

Date and Time	7th July, 1990 9 : 40~14 : 00
Place	Test Field of Japan Sea (3Km offshore from land)
Conditions	Water depth : 41m Displacement : 530t, Draft : 5. 5m Used weight : 6. 8t Slackly moored condition by 6 chain lines
Motion modes	Roll, Pitch, Surge, Sway, Heave (fail)
Test methods	Surge, Sway : by towing due to tub boat Roll, Pitch : by inclination due to additional weight
Measuring Methods	Surge, Sway : Ultrasonic type measuring system Roll, Pitch : Vertical Gyroscope
Environmental Conditions	Significant wave height : about 0. 4m Mean wind velovity and Direction : 3m/sec. NW Gurrent speed : 6cm/sec~7cm/sec

Surge and sway forced oscillation tests were carried out under the condition that β was constant. Table 4.3 shows the condition of the forced oscillation tests.

Analysis method of experiments

1) Representation of viscous drag force

In general, viscous drag forces of surge and sway motions can be represented by

$$F = n_2 \dot{X}|\dot{X}| \tag{4.1}$$
$$n_2 = \frac{1}{2} C_d \rho S$$

Table 4.2 Free decaying test conditions

		surge	sway	roll	pitch
β	at sea	1.3×10^5	1.1×10^5	5.2×10^5	6.6×10^5
	model	9.4×10^2	8.4×10^2	3.0×10^3	3.9×10^3
T_0 (sec)	at sea	70.0	84.7	18.0	14.3
	model	13.4	15.0	3.61	2.77
intial displacement	at sea	7 (m)	8 (m)	3,1.5 (deg)	1.5 (deg)
	model	0.2 (m)	0.2 (m)	7 (deg)	7 (deg)

Table 4.3 Forced oscillation test conditions

	surge			sway		
period (sec)	12	14	16	15	17	19
amplitude (cm)	4~28	4~28	4~28	4~28	4~28	4~28
temp. (℃)	15	15	15	15	15	15
$\nu * 10^{-6}$ (m^2/sec)	1.14	1.14	1.14	1.14	1.14	1.14
Kc	2~14	2~14	2~14	2~14	2~14	2~14
Re * 10^3	2~15	1.8~13	1.6~12	1.8~13	1.6~11	1.4~10
β	1054	903	790	843	744	665

Represlntative length defined of Re or Kc : 0.12 (m)
Projective area defined of Cd : 0.3168 (m^2)

where S is the projection area and C_d denotes the drag coefficient. C_d is said to be a function of Re and K_c numbers or of β and K_c number if roughness can be neglected.

Thus, in case that β is constant, namely the oscillation period is constant, we can regard such coefficient as a function of K_c number only.

In case of forced oscillation tests under a constant period, Re and K_c numbers and β are defined as:

$$K_c = \frac{X\omega_0 T}{D} = \frac{VT}{D}$$
$$R_e = \frac{X\omega_0 D}{\nu} = \frac{VD}{\nu}$$
$$\beta = R_e/K_c = \frac{D^2}{\nu T} = \text{const.}$$

where T is the period of forced oscillation, X is the amplitude and $X\omega_0 = V$ denotes the maximum velocity of oscillation. ν is the fluid viscosity and D is the mean diameter of each column; i.e. 3.0 m at sea and 0.12 m for model.

In case of free decaying tests, since the fluid phenomenon is unsteady, both K_c and R_e numbers change with time. If we assume the free decaying displacement as

$$X = P(t)\sin\omega_0 t; \tag{4.2}$$

then, using the instantaneous velocity amplitude $\sqrt{\dot{P}^2 + \omega_0^2 P^2}$, we can define K_c and R_e numbers as

$$K_c = \frac{T\sqrt{\dot{P}^2(t) + \omega_0^2 P^2(t)}}{D}$$
$$R_e = \frac{D\sqrt{\dot{P}^2(t) + \omega_0^2 P^2(t)}}{\nu}$$

When the variation of period is very small, namely, if the damping force is not so strong, β becomes constant and the drag coefficient may be treated as a function of the time dependent K_c number only, defined by the above equation.

Assuming that the viscous damping moments of pitch and roll motions are directly proportional to angular velocities of motion because of small initial inclinations, we can define damping coefficients of angular motions as

$$N_i = n_i\dot{X}_i, \quad (i = 4, 5) \tag{4.3}$$
$$n_i = 2\zeta_i\omega_{0i}I_i$$

where I_i are the total inertia moments including the added inertia moments.

2) Estimation methods from experimental data

There is now a number of techniques available for processing free-decay data. It involves fitting a parametric model of the damping to the data, usually in a least square sense. The

most common method is an analysis of the envelope of the response, based on the *Krylov* and *Bogoliubov* method [11]. (A generalized form of this method has been developed by *Roberts* [12].)

Recently, regarding the parametric identification methods which can be successfully applied to the problem of estimating the damping parameters, two methods are newly developed by *Roberts et al.* [13]. The one is the state variable filter method and another is the invariant imbedding method.

Here, a new identification method which is based on time series fitting method using a nonlinear optimization technique is developed and applied to the measured free-decay data and the accuracy of this method is evaluated through numerical comparison among the Roberts' results and the present ones (see Fig. 4.1). Comparisons with experimental data are also carried out.

The basic idea of the present method is to identify parametrically each coefficients in a given model equation so as to minimize the square error of the free decay data against a numerical solution of the model equation. As an optimization technique, we used the *Powell* method [14], a kind of nonlinear programing method. This method is that for obtaining the value minimizing an evaluation function defined in a parameter space.

Three coefficients in the model equation, an initial displacement, velocity and a offset of data are parameters to be estimated. The reason why we applied this method to estimate the coefficients in the model equation is that available data for analyzing were gotten up to three periods at most. That is, the meaningful result can not be obtained using the usual analysis method in case of such short data.

In order to confirm the accuracy and the availability of the present method to short free-

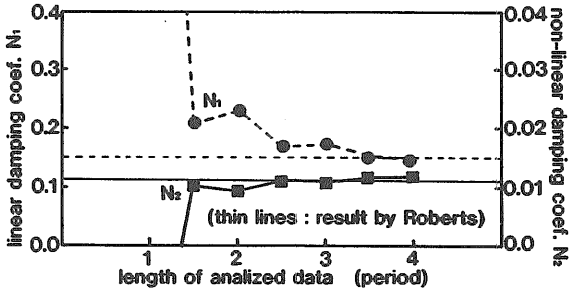

Fig. 4.1 Comparison between the present identification result and the identification one by *Roberts*[13] with respect to estimation of damping coefficients from ship roll data
(In this case, the damping force model is assumed as; $N_1\dot{X} + N_2\dot{X}|\dot{X}|$)

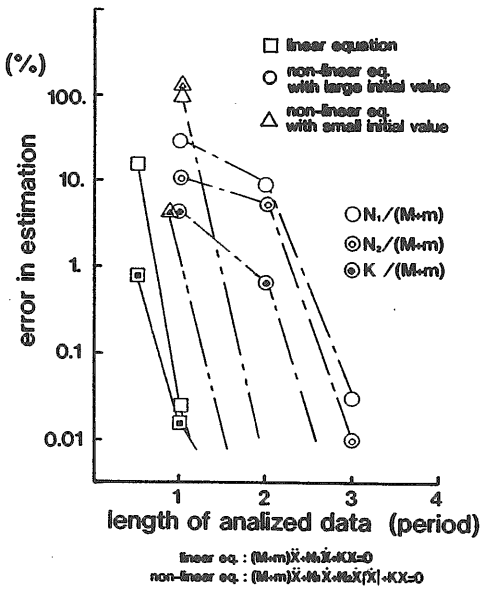

Fig. 4.2 Estimation error

decay data, we compare the known coefficients with the analyzing results due to the present method by using a given equation of motion with nonlinear damping. The estimation error of both is shown in Fig. 4.2.

This figure shows that the present estimation method has a good accuracy even for only three-period-decay data.

While the estimation method of hydrodynamic coefficients from forced oscillation tests is established. Those coefficients, which are equivalently linearized, can be determined from Fourier analysis of forced oscillation reaction force and amplitude.

3) Hydrodynamic coefficients of surge and sway motions

As a free-decay equation of motion, firstly, we assume that the following equation holds:

$$(M+m)\ddot{X} + 0.5\rho C_d S\dot{X}|\dot{X}| + KX = 0 \tag{4.4}$$

$$C_d = \frac{A}{K_c} + B + C \cdot K_c, \quad A, B, C : \text{unknown parameters}$$

where ρ is the fluid density, S is the projection area and $(M+m)$ indicates the virtual mass including the added mass m. This assumption is derived by the following results:

- Figure 4.3 shows the added mass coefficients in low frequencies, obtained from the forced oscillation test in model. It shows that the added mass coefficients can be approximated as constant values at the long periods over 12 sec. (60 sec. at sea).

- According to the calculation based on the three dimensional source distribution method (640 facets), the non-dimensional wave radiation damping coefficient $N/\rho\nabla\omega$ lies in the order of 0.001. Thus, it can be neglected.

- Figure 4.4 shows the static mooring force characteristic in surge motion, obtained from the present time series fitting method under the assumptions that the nonlinear damping force is expressed by a quadratic velocity model with a constant coefficient and the nonlinear restoring force is represented by a linear-plus-cubic displacement model. This figure shows that the restoring force can be approximated as a linear force. And Fig.4.5 shows comparison between measured free decaying time history and simulation one. This simulation is obtained under the situation that the damping coefficient C_d is constant. Both results do not agree. In case of the approximate solution for the drag coefficient of a oscillating cylinder under the assumption that the flow around the cylinder is laminar and two dimensional, so-called *Wang*'s solution [15], it is said that the drag coefficient is in inverse proportion to the *Keulegan-Carpenter number*. Thus it is expected that the damping coefficient includes a component inversely proportional to the K_c number.

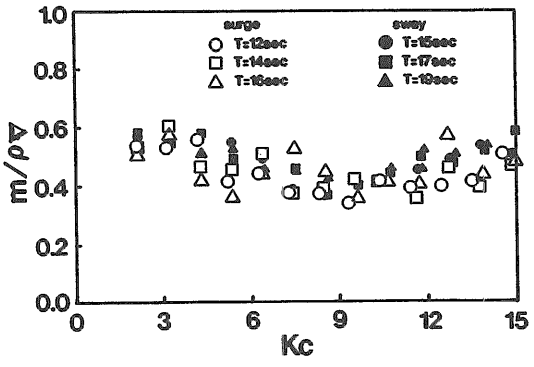

Fig. 4.3 Surge added mass coefficient obtained from forced oscillation test of "POSEIDON" model
(The horizontal axis is the *Keulegan-Carpenter* number, ∇ indicate the displacement of model and ρ is the water density)

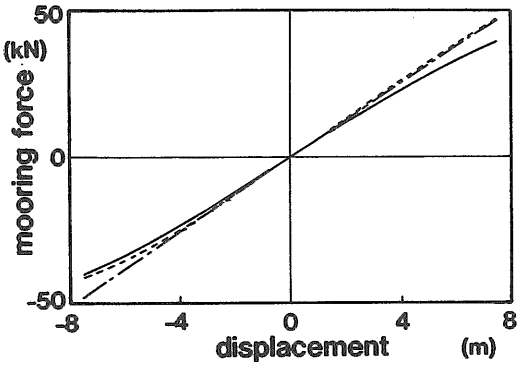

Fig. 4.4 Identified mooring force characteristics of "POSEIDON " at sea

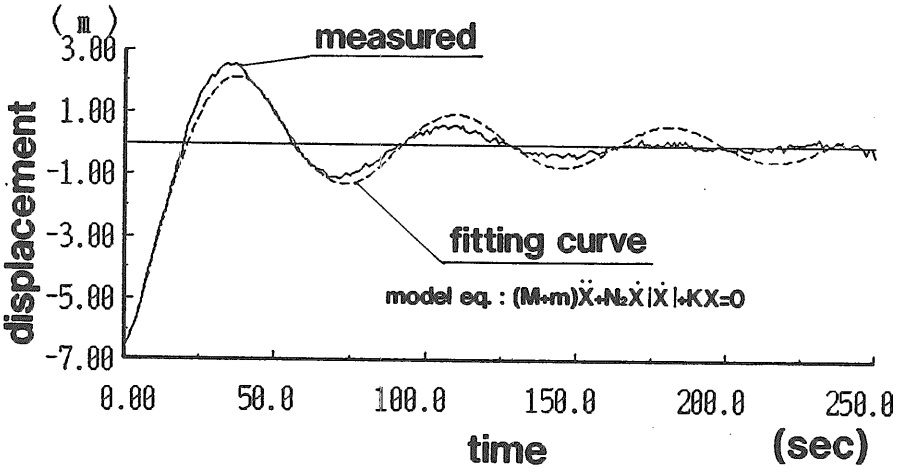

Fig. 4.5 Comparison between full-scale surge decaying time history and the simulation result obtained from the present identification method under the assumption that the drag coefficient is constant and does not depend on the *Keulegan-Carpenter* number

In Eq.(4.4), the number of unknown parameters are five. But since the nonlinear optimization method used to estimate them depends strongly on the initial values for the evaluation function having many minima(i.e. the square error has many minima if there exist many nonlinear terms including unknown parameters.), firstly we determined the undamped natural frequency $\omega_0 = \sqrt{\frac{K}{(M+m)}}$ and assuming that its coefficient is constant, we obtained the parameters A, B and C , i.e. the damping coefficient C_d.

Figures 4.6 and 4.7 show the relations of C_d to K_c numbers for the surge and sway motions. The thick lines are the results of the at-sea free decay tests, the thin ones are

those of the model tests and the marks indicate the results from the forced oscillation tests of the model.

It seems that C_d is inversely proportional to K_c on the whole and that it approaches a constant value with an increase of K_c. This tendency appears in the results presented by *Kinoshita et al.* [16]

Regarding the difference between model and at-sea tests, the damping coefficient of the prototype is larger than one of the model in low K_c numbers while both coefficients are in good agreement in high K_c numbers. Hence we have to take into account the K_c dependence of the damping coefficient to simulate the surge and sway motions including short-period-small-amplitude motions due to waves.

In practice, we can treat the K_c dependence of the damping coefficient as a linear-plus-quadratic velocity model with constant coefficients because if the component proportional to K_c number in C_d can be neglected, C_d becomes $C_1/|\dot{x}| + C_2$ (where C_1 and C_2 are constant values) from the definition of K_c numbers ($K_c = T|x|/D$), that is,

$$0.5\rho C_d S\dot{x}|\dot{x}| = 0.5\rho S C_1\dot{x} + 0.5\rho S C_2\dot{x}|\dot{x}|$$

The first term of the right hand side in the above equation represents a linear damping.

Figure 4.8 shows the comparison of a measured free decay data with the result simulated by this approximate model, where C_1 and C_2 are estimated from the least square fits of the data shown in Figs. 4.6 and 4.7.

Figure 4.8 shows that the approximate simulation model is suitable.

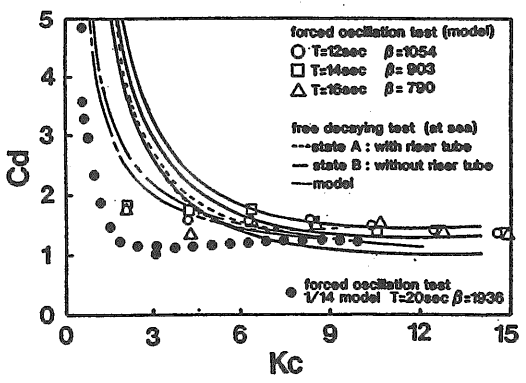

Fig. 4.6 *Keulegan-Carpenter* number dependence of surge drag coefficient (β means the ratio of *Keulegan-Carpenter* and *Reynolds* numbers)

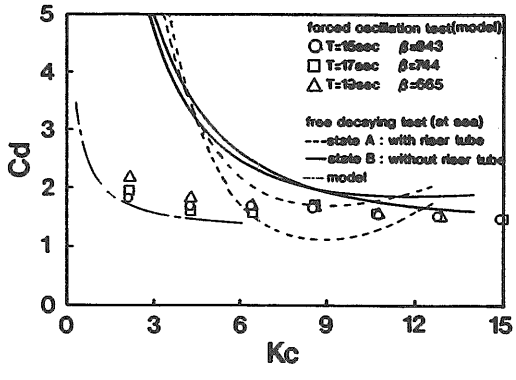

Fig. 4.7 *Keulegan-Carpenter* number dependence of sway drag coefficient

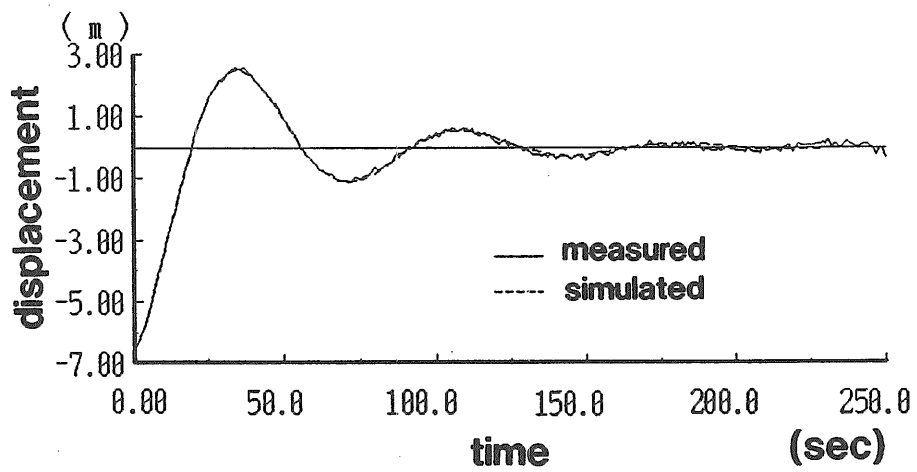

Fig. 4.8 Comparison between full-scale surge decaying time history and the simulation result obtained from the present identification taking into account the *Keulegan-Carpenter* number dependence of drag coefficient

4) Hydrodynamic coefficients of roll and pitch motions

Figures 4.9 and 4.10 show the extinction curves of roll and pitch motions. The marks are the results obtained in the following way:

Let x_n be sequential peak values(amplitudes) of damping curve. If we assume that the decaying motion can be represented by:

$$x = X_0 \exp[-\frac{N^e t}{2I}] \sin(\frac{2\pi t}{T_0} + \Psi) \tag{4.5}$$

where T_0 is the natural period, I the virtual inertia moment, and N^e the equivalent linearized damping coefficient. Then if we plot $\mid x_{n+2} - x_{n+1} \mid$ as a function $\mid x_{n+1} - x_n \mid$ and the damping is constant, from Eq.(4.5) we get:

$$\mid x_{n+2} - x_{n+1} \mid = \exp[-\frac{N^e T_0}{4I}] \mid x_{n+1} - x_n \mid \tag{4.6}$$

Thus, using the least square method, the minimum error estimate of the inclination Θ can be obtained. The natural period T_0 is obtained from the mean of zero-up-crossing periods and zero-down-crossing periods. Then the virtual mass and equivalent damping coefficient are given by:

$$I = \frac{T_0^2 K}{4\pi^2} \tag{4.7}$$

$$N^e = -\frac{T_0^2 K \log(\Theta)}{\pi^2} \tag{4.8}$$

where K is the restoring moment coefficient.

This is the well known extinction curve fitting method. In these figures, circles are the at-sea free decay results and the other marks indicate the model free decay results.

Furthermore the lines indicate the results due to the present method, *i.e.* time series fitting method.

It is found that both analysis results are in good agreement and the model damping coefficients of roll and pitch motions are greater than the at-sea ones.

5) Final results

The at-sea results relating to the hydrodynamic force and stiffness coefficients excluding wave radiation damping forces are summarized in Table 4.4.

As for heave motion, the damping force of a quadratic velocity model with a constant C_d equals to 2.0 and the restoring force due to static water pressure are taken into account. The added mass and wave radiation damping coefficients are obtained from the calculation

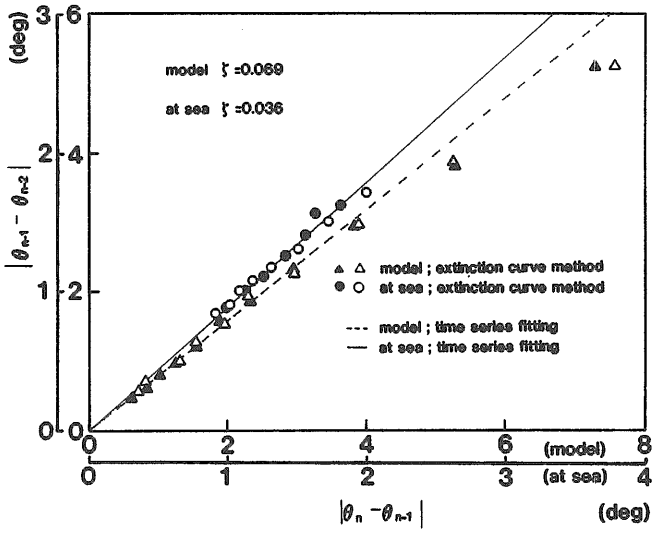

Fig. 4.9 Extinction curve of full-scale pitch decaying motion
(The lines shows the identified lines by the present fitting method and ζ represents the dimensionless linear damping coefficient)

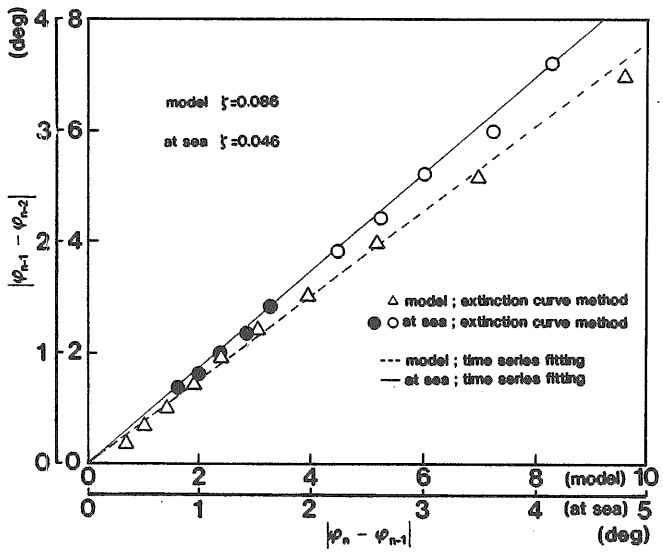

Fig. 4.10 Extinction curve of full-scale roll decaying motion

Table 4.4 Each identified coefficients in motion equation

	inertia	linear damping	nonlinear damping	restoring
unit	kg	N/ (m/sec)	N/ (m/sec)^2	N/m
surge	7.9×10^5	4.3×10^4	3.0×10^4	6.4×10^3
sway	7.9×10^5	5.4×10^4	3.0×10^4	4.4×10^3
heave	9.5×10^5		1.6×10^5	4.5×10^5
unit	kg•m^2	N•m/ (1/sec)	N•m/ (1/sec)^2	N•m
roll	7.8×10^7	2.2×10^6	1.0×10^7	8.3×10^6
pitch	1.4×10^8	1.8×10^6	2.7×10^8	2.6×10^7

based on the three dimensional source distribution method (a number of facets is 640).

4.2 External forces

4.2.1 Wind loads

Not only steady wind loads but also wind fluctuation loads should be taken into account to simulate the equation of motion in time domain.

The wind loads are estimated from the measured wind pressures as follows:

$$F_1^w(t) = \Delta p_1(t) S_1 \quad \text{for downwind direction}$$
$$F_2^w(t) = \Delta p_2(t) S_2 \quad \text{for transverse direction}$$

$\Delta p_i(t), (i = 1, 2)$ are the measured time histories of the wind pressure difference , and $S_i, (i = 1, 2)$ are the projection areas for each directions.

In our simulation, the wind loads are taken into account only for surge and sway motions.

4.2.2 Wave loads

First and second order forces are taken into account to simulate the time histories of the motion. And we assume that the effect of second order potential to the second order forces and the nonlinearity higher than third order of incident waves is negligible, and the incident wave system can be considered as an unidirectional wave system.

The time histories of incident waves are synthesized using wave data by the ultrasonic wave gauges installed on the sea bottom, the relative wave height meter and the accelerometer on the deck. The data by the ultrasonic wave guages are used as an amplitude information and the ones by the relative wave meter are done as a phase information.

Furthermore we tried to analyze a phase difference of both wave data. As a result, we could get the phase difference equivalent to the distance 194 m. This value was close to the value 180 m measured by divers at a calm sea.

As found in Fig.3.5, the main direction of incident waves is some degree starboard direction. This is obvious from Fig.3.7 because the sway spectra have a significant wave power. However, the accuracy of directional wave data by wave guages installed like a line array on the sea bottom is not so good and the objective of this simulation is to confirm whether the slow drift surge and sway motions can be simulated under a rough environmental condition. Thus, we dare consider the main direction of wave and wind head.

We shall investigate the characteristics of slow drift force at sea.

The amplitude of QTF(Quadratic transfer function) of surge slow drift force is shown in Fig.4.11, which is obtained from numerical calculations. In this figure, Ω_1 means the mean wave frequency of two wave components and Ω_2 denotes the difference wave frequency between them.

This figure shows that there exists a peak in the vicinity of $\Omega_1 = 1.7$ rad/sec. and the amplitude of QTF changes slowly around it.

In order to compare this numerical results with the measurements at sea, we carry out

a cross bi-spectral analysis. The cross bi-spectral analysis followed the Dalzell's work [17]. On the analysis, there are two problems in this case. The one is if waves and wind fluctuation are mutually independent in statistical sense and another is if wind fluctuation is Gaussian distributed. However, as shown in Appendix A, we assume that wave and wind fluctuation processes are independent mutually and that wind fluctuation is the Gaussian process.

And we note that a QTF obtained from such analysis is just that of surge response, G_2. Thus the transform it to the QTF of second order force G_2^f may be given by:

$$G_2^f(\omega_1, -\omega_2) = G_2(\omega_1, -\omega_2)/H_L(\omega_1 - \omega_2) \tag{4.9}$$

where H_L is the linear transfer function of surge motion to the external force, which is obtained from the free oscillation test in still water if the hydrodynamic force coefficients do not change in waves and it may be given by:

$$H_L(\omega) = \frac{1}{K - (M+m)\omega^2 + iN^e\omega} \tag{4.10}$$

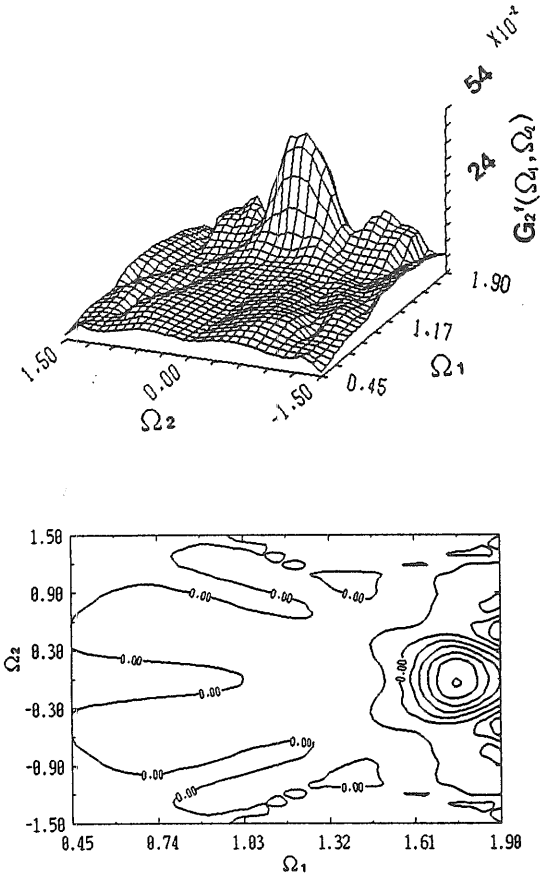

Fig. 4.11 Calculated QTF(Quadratic Transfer Function) of second order slowly varying drift force (Ω_1 and Ω_2 mean the mean and difference frequencies of two wave components)

Figure 4.12 a) shows the QTF of second order force at $\Omega_2 = 0$, i.e. frequency characteristics of steady drift force. Figure 4.12 b) indicates the amplitudes of the QTF of second order force vs. the difference frequencies, Ω_2. The results of model tests are also shown in Fig.4.12 a). Black circles are the results obtained from the 1/14.3 model tests in regular waves and the broken line is the ones obtained from the numerical values taking account of the effect of viscous drift force, which was presented in the previous paper [4]. The horizontal axis indicates the mean frequency of different two wave components. In Fig.4.12 b) there exist five theoretical lines for each Ω_2, but the differences among them are too small to be indicated in the figure.

From this figure the numerical result based on the potential theory is much lower than the experimental ones, but both results have the same tendency. That is, the amplitudes of QTF of second order force against the difference wave frequency increase gradually with

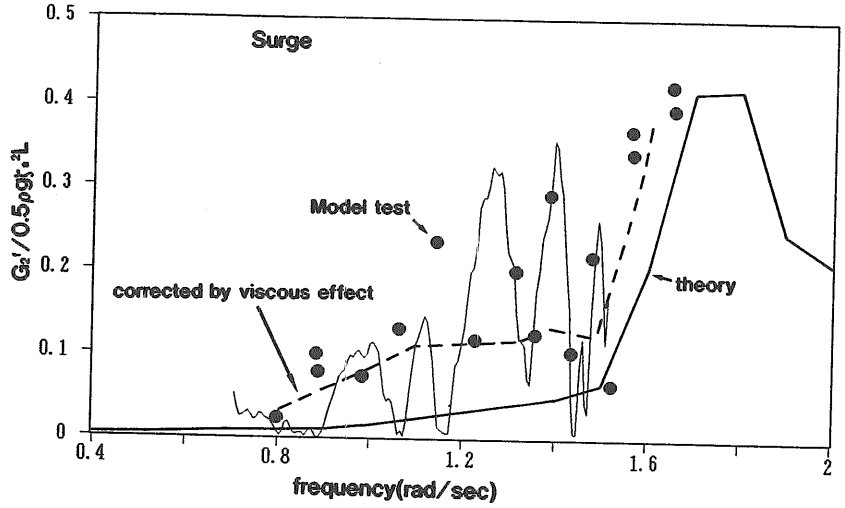

Fig. 4.12 a) Steady drift force coefficient to wave frequency $\omega(=\Omega_1)$
(Legend: ●; model test results, thin line; full-scale experimental result obtained from the cross bispectral analysis, bold solid line; theoretical line based on the second order potential theory, dash-dotted line; theoretical line corrected by viscous effect)

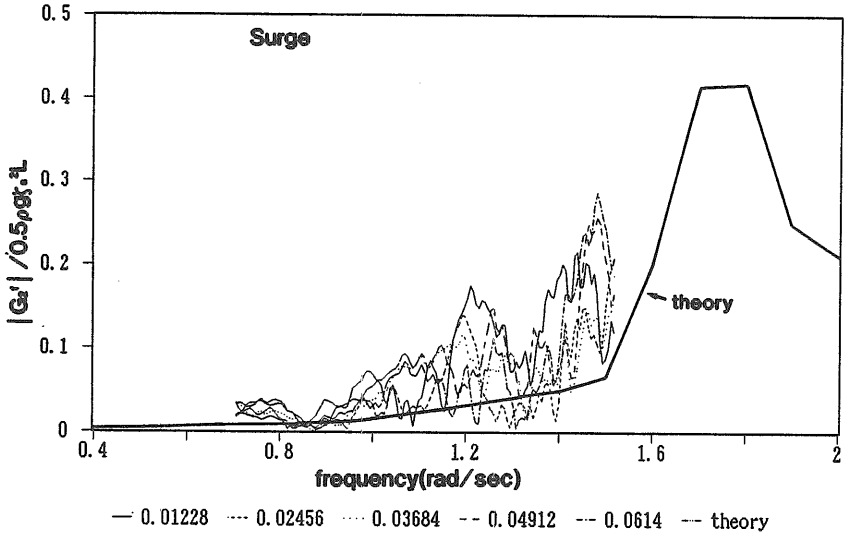

Fig. 4.12 b) Amplitude of QTF of second order slow drift force to mean wave frequency Ω_1 of two wave components
(Legend: thin lines; full-scale experimental results to each difference frequencies of two wave components, solid line; theoretical lines)

an increase of the mean wave frequency. And concerning steady drift force, the broken line, i.e. the corrected numerical result taking into account the effect of viscous drift force, agrees with not only model test results but also at-sea experimental ones. It is concluded that in order to estimate the QTF of second order force of the floating structure consisting of many circular slender legs, we should take not only the potential drift force but also the viscous one into account.

4.3 Simulation model

A simulation model dealt with is as follows:

$$\sum_{i=1}^{5}(M_{ki}+m_{ki}(\infty))\ddot{X}_i+\int_{-\infty}^{t}\mathrm{K}_{ki}(t-\tau)\dot{X}_i d\tau+N_{ki}^{(1)}\dot{X}_i+N_{ki}^{(2)}\dot{X}_i|X_i|+(a_{ki}+b_{ki})X_i$$
$$=F_k^{(1)}(t)+F_k^{(2)}(t)+F_k^{w} \tag{4.11}$$

where

- M_{ki} ; Mass matrix
- $m_{ki}(\infty)$; Added mass matrix at $\omega=\infty$
- $N_{ki}^{(1),(2)}$; Viscous damping coefficient matrix.
- a_{ki} and b_{ki}; Stiffness matrix due to static water pressures and mooring line force respectively.
- K_{ki}; Memory effect function matrix
- $F_k^{(1),(2)}$; First and second order force column vector. A double summation method is used to get time histories of such force.
- F_k^{w}; Wind force column vector. Only the components in surge and sway motion directions are taken into account.

As a simulation condition, we use equations of five mode coupling motion excluding yaw motion in order to take the occurrence of sway motion due to wind and other motion modes into account.

As an estimate of the QTF of second order force, judging from the difference between the results of at-sea experiment and the numerical calculation, we adopted about twice values of the calculated QTF.

4.4 Results and discussion

Figure 4.13 shows a comparison between the simulated time history and measured one. Figure 4.14 shows the spectra of both results.

Both results are in rough agreement but, as for the phase of slow drift motion, they are slightly different. It is considered that this discrepancy is due to the uncertainties of the phase information of the QTF of second order force.